Rockfall rebound: comparison of detailed field experiments and alternative modelling approaches

Franck Bourrier, Frédéric Berger, Pascal Tardif, Luuk Dorren, Oldrich Hungr

Rockfall rebound: comparison of detailed field experiments and alternative modelling approaches

Franck Bourrier,[1]* Frédéric Berger,[1] Pascal Tardif,[1] Luuk Dorren[2] and Oldrich Hungr[3]

[1] Cemagref, UR EMGR, 2 rue de la papeterie, BP 76, Saint Martin d'Heres, FR 38 402, France
[2] Federal Office for the Environment FOEN, Hazard Prevention Division Bern, CH
[3] University of British Columbia, Earth and Ocean Sciences, Vancouver, Canada

ABSTRACT: The accuracy of rockfall trajectory simulations mainly rests on the calculation of the rebound of fragments following their impact on the slope. This paper is dedicated to the comparative analysis of two rebound modelling approaches currently used in rockfall simulation using field experiments of single rebounds. The two approaches consist in either modelling the rock as a single material point (lumped mass approach) or in explicitly accounting for the fragment shape (rigid body approach). A lumped mass model accounting for the coupling between translational and rotational velocities and introducing a slope perturbation angle was used. A rigid body approach modelling the rocks as rigid locally deformable (in the vicinity of the contact surface) assemblies of spheres was chosen.

The comparative analysis of the rebound models shows that both of them are efficient with only a few parameters. The main limitation of each approach are the calibration of the value of the slope perturbation ('roughness') angle, for the lumped mass approach, and the estimation of the rock length and height from field geological and historical analyses, for the rigid body approach. Finally, both rebound models require being improved in a pragmatic manner to better predict the rotational velocities distribution.

Introduction

Rockfall hazard assessment is now routinely quantified using rockfall trajectory simulation codes. Among the four basic types of movement, flight, rebound, sliding, and rolling, most often only the first two are considered quantitatively.

Modelling the process of impact and rebound using physically consistent and field applicable approaches is one of the most difficult tasks in developing these codes. One can differentiate two general types among these approaches: modelling the rock as a single material point or explicitly accounting for the fragment shape. Both of these approaches have been shown to be able to provide representative results on different study sites (Labiouse *et al.*, 2001; Guzzetti *et al.*, 2002; Dorren *et al.*, 2006). However, in most cases, the accuracy of the approaches is only evaluated by comparative analysis of the stopping points of the rocks because the kinematics of the passing rocks cannot easily be quantified from analysis of past events. Consequently, calibration of models does not generally include this data. Only a few experiments have ever been done to evaluate the kinematic parameters of falling rocks at specific locations using field experiments (for example, Giani *et al.*, 2004; Dorren *et al.*, 2006; Bourrier *et al.*, 2009a). Even in the few published detailed field studies most report only measurements of the translational velocities of the rocks. Several researchers made more complete measurements of fragment rebound kinematics in laboratory experiments (Chau *et al.*, 1998, 2002; Labiouse

and Heidenreich, 2009), but these are difficult to extend to field processes due to the difficulties encountered when defining similitude rules.

The aim of the study presented in this article is to extract from well documented field experiments using video movies a complete description of translational and rotational particle kinematics before and after rebound and to use this data to evaluate the capabilities for two different approaches to model rockfall rebounds.

Study Site and Field Rockfall Experiments

The rockfall experimental site (Figure 1) is located in the 'Forêt Communale de Vaujany' in France (lat. 45°12′, long. 6°3′) (Dorren *et al.*, 2006). The 100 m wide and 570 m long study site covers an avalanche path denuded of trees, ranging in altitude from 1200 m to 1400 m above sea level with a mean slope angle of 38°.

The experiments consisted of releasing rocks down the slope using an excavator. The sizes and shapes of the rock particles were carefully chosen. Priority was given to rocks having nearly parallelopiped shapes and volumes approximately equal to $1.0 \, m^3$. Each rock was measured along its three dominant axes and its volume was estimated from these data. The mean volume of the rocks was $0.8 \, m^3$ and the standard deviation $0.15 \, m^3$. Five digital cameras installed along the slope were used to record rockfall trajectories. Additional details on the experiments can be found in Dorren *et al.* (2006).
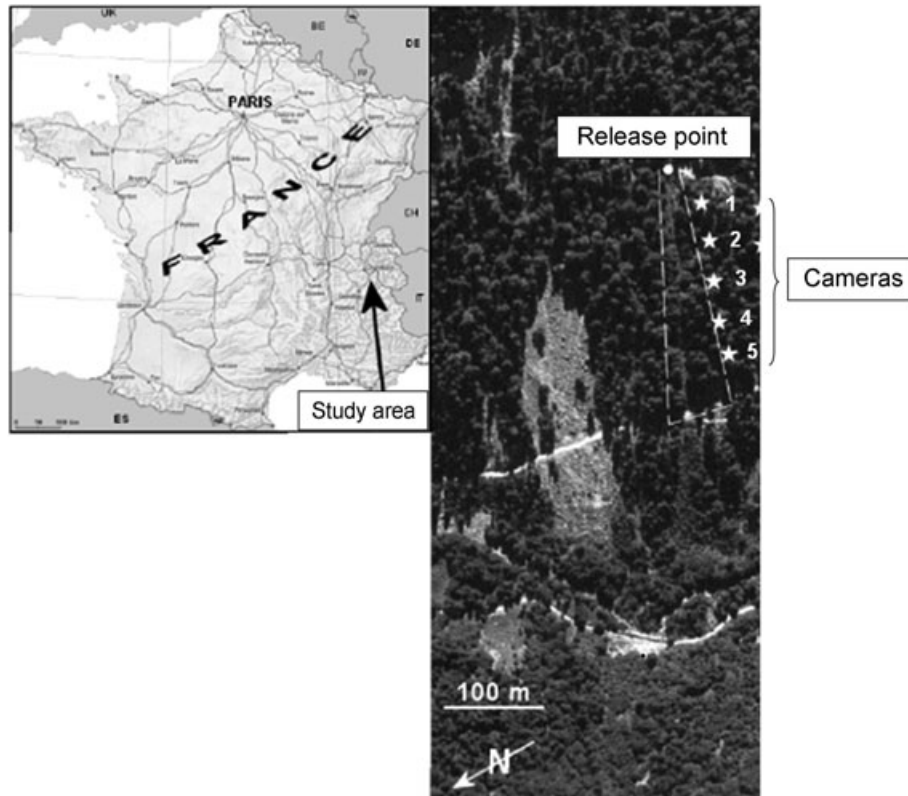
Figure 1. The study site.

Methods

Experimental measurements of particle rebound

This study concentrates on quantifying the kinematical changes of the rocks in the vicinity of their impact point on the slope substrate. Analysis of the digital footage was carried out to determine the trajectories of the particles in the vicinity of identifiable impacts.

For a given impact, the measurement of the trajectory just before a rebound gives the incident translational and rotational velocities. Reflected velocities were obtained by analyzing the trajectory after rebound.

It was not possible to measure all six velocity components in three dimensions using the cameras. One can note that, although it was not the initial aim of the experiments, it might have been possible to measure the trajectories of the rock in 3D if cameras had also been installed perpendicularly to the main direction of rocks propagation (Dewez *et al.*, 2010). However, the analysis of the 3D trajectory of the rocks remains a very difficult task that requires very thorough topographical field work to build a digital terrain model and locate the cameras as well as a precise procedure for the scaling of the distance measured using the different cameras.

The recordings of the cameras were used to measure the projection of the translational velocities in the camera frame and the component of rotational velocity around an axis perpendicular to the camera frame. In order to limit projection errors, only those particles travelling approximately parallel with the plane of the camera frame and rotating in this plane have been chosen for analysis. Only the rocks propagating in the lower part of the main propagation corridor during the complete duration of the film were selected. Their maximum deviation can therefore be evaluated to be less than 5 m, corresponding to half of the corridor width, during a 25 m long propagation, corresponding to the width of the camera frame. Consequently, the maximum deviation angle in the selected films is approximately 11°.

The rejections of films due to strongly deviating trajectories and to non-identifiable impact point strongly reduce the number of rebound observations that can be used in the study. First, the rejection of strongly deviating trajectories leads to the suppression of approximately 10% of the records. Second, the required identification of a clear rebound in the film was a highly selective criterion inducing the rejection of approximately 90% of the records. This identification was difficult due to the predominance of rolling motion in the first phase of the propagation, the various obstacles hiding the rocks propagation, and to difficult identification of the first and last contact time between the rock particle and the slope surface. Finally, the number of rebounds used in the study was limited to 30, although 100 rocks were released and 5 cameras were installed along the slope. Most of these rebounds occurred in the area between 50 and 200 m from the release point.

Frame images were extracted from the films using an image interlocking suppression process for every 1/50th second (Figure 2). Processing of every image allowed determination of the contour of the rock and, as a result, calculation of the location of the gravity centre of the rock and the orientation of the rock in the image. These data had to be converted from pixel units to metric units. The conversion ratio is calculated for each image from measurement of the distance in pixels between specific points whose distances were measured in the field. For each rebound, different point couples were used to estimate the error included in the conversion factor.

The incident and reflected velocities were calculated from linear regressions of the time evolutions of the location of the gravity centre of the rock and of its orientation (Figure 3 and 4). The regression relationships are based on the theoretical equations of the horizontal and vertical motions of a rock under gravity, for free flight phases between impacts (ballistic trajectory). Linear regression of the time evolution of the particle orientation also allowed calculation of the mean rotational velocities of the rock before and after rebound. The calculation process is

Figure 2. Rebound of a rock reconstructed from a serie of successive images extracted from a camera film (50 frames per second). This figure is available in colour online at wileyonlinelibrary.com/journal/espl
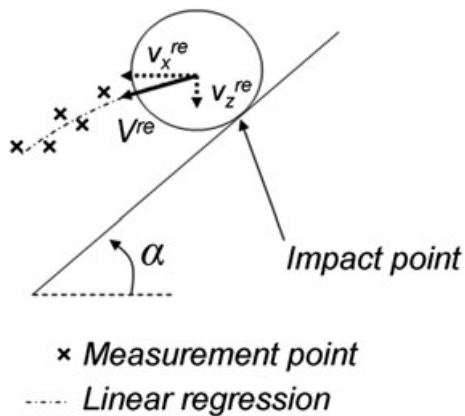

× Measurement point
····· Linear regression

Figure 3. Principle of the analysis of the measurement points using linear regressions to obtain the values of the reflected velocities.

illustrated for reflected velocities. The theoretical trajectory of the rock gravity centre just after rebound is characterized by the equations (Figure 4):

$$X(t) = v_x^{re} t \qquad (1)$$
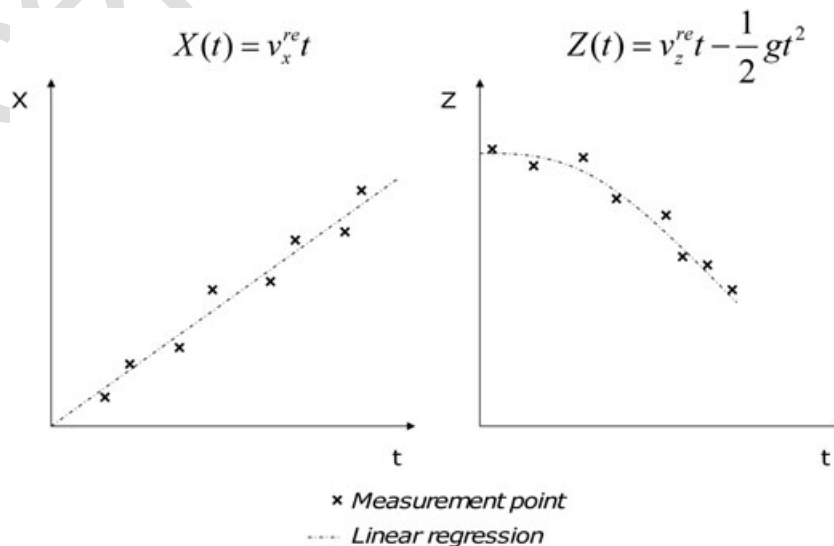
$$Z(t) = v_z^{re} t - \frac{1}{2} g t^2 \qquad (2)$$

where $X(t)$ and $Z(t)$ are the horizontal and vertical positions of the rock gravity centre, v_x^{re} and v_z^{re} are the horizontal and vertical components of the reflected velocities, g is the gravitational acceleration, and t is the time starting from the end of the previous impact on the soil.

The components of the rock velocity tangential (v_t^{re}) and normal (v_n^{re}) to the slope surface are calculated from the horizontal and vertical components:

$$v_t^{re} = v_x^{re} \cos \alpha - v_z^{re} \sin \alpha \qquad (3)$$

$$v_n^{re} = v_x^{re} \sin \alpha + v_z^{re} \cos \alpha \qquad (4)$$

where α is the mean slope angle in the vicinity of the current particle position (Figure 3).

The error on the measured velocities can be decomposed into the error in the value of the conversion factor from pixel to metric unit and the rock gravity centre identification error resulting in the regression error. The errors were quantified by indirect methods to estimate the accuracy of the velocity measurements. The conversion factor was calculated for one image using 10 different known field point couples. The maximum difference in the calculation of the conversion factor is 6.3% of the minimum values of the factor. To estimate both the regression error and the error on the rock gravity centre identification, the same footage was treated 10 times. From these 10 measurements, the mean regression residual is of the order of 0.05 m and the maximum difference between the norm of the velocities is 9.1% of the maximum velocity obtained.

Rebound modelling approaches

Rockfall models simulate the propagation of the rocks through a given study site. The site slope surface can be approximated in 2D by a slope profile, or in 3D by, for example, a rasterized digital elevation model. Whatever the rockfall simulation approach chosen, the free fall of the rocks is explicitly modelled by the ballistic parabola with an initial velocity. After each parabolic free fall, the intersection between the rock trajectory and the slope surface is detected and consequently a rebound model allows calculation of the reflected translational and rotational velocities. Rebound models can be separated into two types (Guzzetti *et al.*, 2002; Dorren, 2003): lumped-mass

× Measurement point
····· Linear regression

Figure 4. Linear regressions for the derivation of translational velocity components.

and rigid body models. In this study, both types have been tested. The inputs of both of these models are the components of the incident velocities and the outputs are the components of the reflected velocities. For incident and reflected velocities in three dimensions, there are six components: three translational velocities and three rotational velocities.

However, because the field measurements were limited to their 2D projections, as discussed earlier, two-dimensional versions of the analytical models were used, with three velocity components for incident and reflected velocities. These components are the tangential v_t^{in} (resp. v_t^{re}), the normal v_n^{in} (resp. v_n^{re}), and the rotational ω^{in} (resp. ω^{re}) incident (resp. reflected) velocities (Figure 5).

Lumped-mass approach

This study uses only non-deviating interactions, where both the incident velocity plane and the reflection plane are approximately vertical and parallel, lying in the camera frame, i.e. δ^{re} in Figure 6 is assumed equal to zero.

Lumped-mass approaches consider the falling rocks as a moving material point, bearing linear and in some cases also rotational momentum. Geometrical and mechanical properties are also associated with the local slope surface in the neighbourhood of the impact point. Among the numerous rebound calculation models (Piteau and Clayton, 1977; Wu, 1985; Bozzolo and Pamini, 1986; Descoeudres and Zimmermann, 1987; Bozzolo et al., 1988; Spang and Rautenstrauch, 1988; Paronuzzi, 1989; Pfeiffer and Bowen, 1989; Fornaro et al., 1990; Kobayashi et al., 1990; Giani, 1992; Evans and Hungr, 1993; Budetta and Santo, 1994; Azzoni et al., 1995; Spang and Sonser, 1995; Kamijo et al., 2000; Ushiro et al., 2000; Guzzetti et al., 2002; Bourrier et al., 2009b), we chose to use a model based on the classical restitution coefficient approach, which also allows one to account for the coupling effects
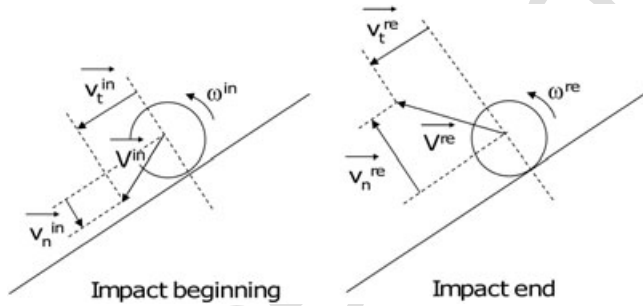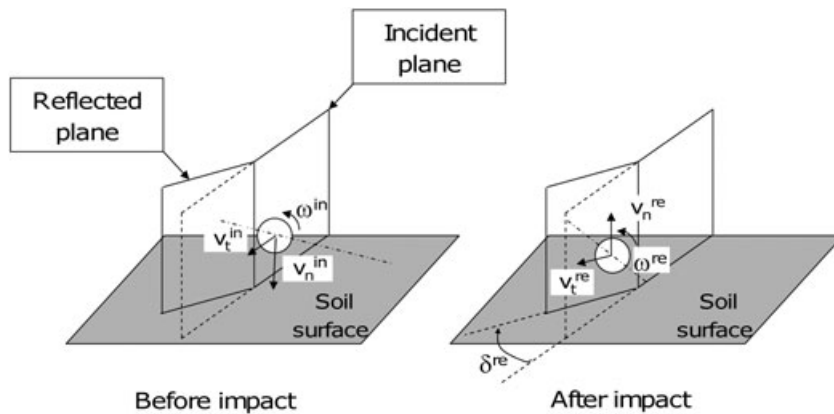
between the translational and rotational velocities of the rocks (Bourrier and Hungr, 2011). This coupling is introduced using the equations (Goldsmith, 1960) describing the collision of a spherical body with a planar surface. The changes in the normal impulse of the rock during the impact are related through a coefficient of normal restitution, r_n. In a modification of the original Goldsmith equations, the tangential impulse at the contact point is also reduced by a tangential restitution coefficient r_t. The functional relationships between the reflected and incident velocities depend on the value of a friction limit angle γ compared with the contact friction angle φ:

$$\tan \gamma = \frac{2\left(r_t v_t^{in} + R r_t \omega^{in}\right)}{7 v_n^{in}(1 + r_n)} \tag{5}$$

where R is the equivalent radius of the rock.

If the friction limit angle γ is smaller than the friction angle φ, no slip occurs at the contact and the only energy loss sources are associated with the two restitution coefficients. Thus, if $\varphi > \gamma$:

$$\begin{vmatrix} v_t^{re} \\ v_n^{re} \\ R\omega^{re} \end{vmatrix} = \begin{vmatrix} \frac{5}{7}r_t & 0 & -\frac{2}{7}r_t \\ 0 & -r_n & 0 \\ -\frac{5}{7}r_t & 0 & \frac{2}{7}r_t \end{vmatrix} \times \begin{vmatrix} v_t^{in} \\ v_n^{in} \\ R\omega^{in} \end{vmatrix} \tag{6}$$

On the contrary, if the friction angle exceeds the friction limit, frictional energy dissipation is considered at the contact point. If $\varphi < \gamma$:

$$\begin{vmatrix} v_t^{re} \\ v_n^{re} \\ R\omega^{re} \end{vmatrix} = \begin{vmatrix} r_t & -\tan\phi(1 + r_n) & 0 \\ 0 & -r_n & 0 \\ 0 & -\frac{5}{2}(1 + r_n) & r_t \end{vmatrix} \times \begin{vmatrix} v_t^{in} \\ v_n^{in} \\ R\omega^{in} \end{vmatrix} \tag{7}$$

The main specificity of the model is the calculation of the normal restitution coefficient r_n from the incident normal momentum M_n^{in}, equal to mv_n^{in} with m the mass of the rock, using a hyperbolic relationship:

$$r_n = \frac{M_{0.5}}{M_n^{in} + M_{0.5}} \tag{8}$$

where $M_{0.5}$ is the reference momentum that is the normal momentum in an impact in which the restitution factor r_n equals 0.5.

The hyperbolic function (Equation (8)), controlled by only one coefficient: $M_{0.5}$, equals 1.0 in very light impacts, where the response of the materials may remain almost completely

Figure 5. Incident and reflected velocity components in 2D.

Figure 6. Deviation of the incident and reflection planes (neglected in this analysis).

4

elastic, but would tend to zero in extremely heavy ones, where all the energy is lost in plastic deformation.

Finally, a local slope perturbation angle α_l (Figure 7) is substracted from the mean slope angle calculated from the digital elevation model, so that the local roughness of the soil could be implicitly accounted for.

As the rebounds observed in the field experiments were measured along a part of the slope with very constant soil properties, the choice was made to set the restitution coefficient and the friction angle associated with the soil properties at fixed values. On the contrary, the local changes in the local slope surface are obviously dependent on the location of each impact point. For that reason, the local perturbation in the angle α (Fig. 7) was extracted from a uniform distribution ranging between zero and a maximum angle α_l^{max}: $\alpha_l \in [0, \alpha_l^{max}]$. The calibration parameters of the model are therefore limited to four: $M_{0.5}$, r_t, φ, and α_l^{max}.

Rigid body approach

In contrast to lumped mass models, some rockfall trajectory simulation codes explicitly account for the shape of the rock and for the contact point location. In these approaches, the interaction forces between the rock and the soil are applied at a contact point corresponding to the gravity centre of the contact surface. The 2D or 3D translational and rotational velocities of the rock are explicitly accounted for based on Newton's equations, solved using either non-regular mechanical approaches (Moreau and Panagiotopoulos, 1988; Frémond, 1995; Brogliato, 1999) or regularized methods such as the discrete element method (Cundall and Strack, 1979). Both regularized and non-regular approaches can account for complex shapes, incident kinematics and for energy dissipation within the soil forming the slope surface. In this study, the discrete element method has been used. The reflected velocities are calculated from the incident velocities using an explicit iterative solution scheme. At each time step, the forces applied by the soil to the particle are calculated from the location of the rock and the velocity of the contact point. Contrary to classical non-regular approaches (Moreau and Panagiotopoulos, 1988; Frémond, 1995; Brogliato, 1999), the rocks are not considered to be rigid bodies but rigid, locally deformable (in the vicinity of the contact surface), bodies. Such an approach can, however, be considered as a rigid body approach in the sense that it allows directly accounting for the shape of the rocks.

In the code, the particle is simulated as an unbreakable assembly of spheres (Nicot et al., 2007). This approach provides important advantages with regard to the efficiency of the numerical solution. The detection of a contact between a surface and a sphere is much easier than the detection between a polyhedron and a surface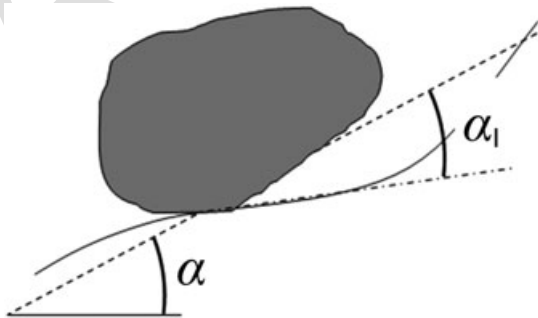. Only one contact type has to be treated for sphere/plane contact, whereas, for polyhedron/plane contacts, three contact types should be introduced (face–face, edge–face and vertex–face). In addition, available mechanical models for the calculation of interaction forces between a sphere and a surface are more numerous.

A number of interaction models of varying complexity exist that are able to account for the elastic interaction and for plastic, frictional or viscous energy dissipations at the contact point (Descoeudres and Zimmermann, 1987; Dimnet and Frémond, 2000; Di Prisco and Vecchiotti, 2006; An and Tannant, 2007; Salciarini et al., 2009). A simple elasto-plastic model was chosen for this study, in order to limit the required number of calibration parameters. In the model chosen, two parameters are related with the elasticity of the two materials in contact. These parameters are the elastic compression modulus E and the Poisson ratio v. One parameter r_k is associated with the plastic energy dissipation along the normal to contact direction. This parameter can be related with the ratio between the loading and the unloading modulus during classical load plate tests. Finally, the Coulomb friction angle φ_c allows quantification of the frictional energy dissipation along the tangent to the contact surface. Thus, there are only four calibration parameters, comparable with the lumped-mass approach. However, in this approach the shape and the orientation of the particle just before the interaction are explicitly accounted for and have to be defined for each rebound simulation.

Although the rigid body approach allows direct computation of the rebound in 3D, the comparison with the measurements required setting up the incident velocities and collecting the reflected velocities in a 2D frame corresponding to the camera frame. To simulate the experimental rebounds, the rocks were modelled as assemblies of two interlocked spheres. The shape of each particle was characterized by its height and length (Figure 8). These quantities were related with the diameters and distances of the spheres, respectively. For each rebound, simulated heights and lengths of the particles were set corresponding to the minimum and maximum lengths of the real rocks, as measured in the field. Because the orientation of the particles immediately before impact (Fig. 8) is unknown and could not be measured in the experiments, it was assumed to be a random quantity represented by 19 equally distributed values of the angle β covering the range of all possible orientations ($0° \leq \beta < 180°$).

Each rebound simulation consisted in first setting the rock height, length, and orientation following the above mentioned methodology. Second, the model of the rock was built just before impact and the measured incident velocities were set

Figure 7. Concept of slope perturbation angle α_l, representing roughness, substracted to the mean slope angle α.
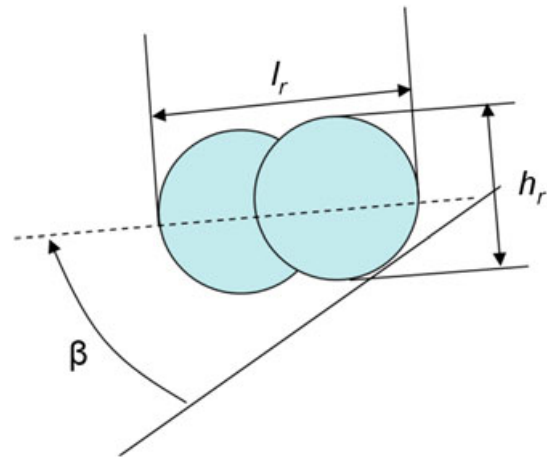

Figure 8. Definitions of the particle length l_r, height h_r and orientation angle β. This figure is available in colour online at wileyonlinelibrary.com/journal/espl

up as initial conditions. Third, the simulation was launched. Finally, reflected velocities were collected at the end of the rebound, defined as the time when a sign change in the normal to soil surface velocity was observed.

Thus each of the two models contains a small number of fixed parameters, to be determined by trial-and-error calibration (Table II) and one random parameter controlled by a uniform distribution: the roughness perturbation angle for the lumped mass model and the particle orientation angle for the rigorous model. The results of the calculations are to be evaluated by observing the statistical distributions of the reflected velocities, in comparison with the distribution of velocities measured in the experiments.

Results and Discussion

Results of the field experiments

The distributions of the incident and reflected velocities measured in the experiments (Figure 9) first show that the variability of all these quantities is very strong as the range of each measured values is large compared with the corresponding mean value (Table I). In addition, for each velocity component, the distributions of the incident and reflected velocities are fairly similar. The energy exchanges, dissipations, and transfers due

to the rebound are therefore relatively small on average or compensate each other in the rebounds that were selected for use.

These results can also be compared with the values of apparent tangential (R_t^a) and normal (R_n^a) restitution coefficients at the gravity centre of the impacting rocks stated in the literature (Guzzetti *et al.*, 2002; Dorren, 2003). The coefficients R_t^a and R_n^a are defined as follows:

$$R_n^a = v_n^{re}/v_n^{in} \qquad (9)$$

$$R_t^a = v_t^{re}/v_t^{in} \qquad (10)$$

In rockfall literature, classical values for the normal coefficient R_n^a range from nearly nil values to about 0.6 and the

Table I. Mean values and standard deviations of the distributions of the experimental incident and reflected velocities

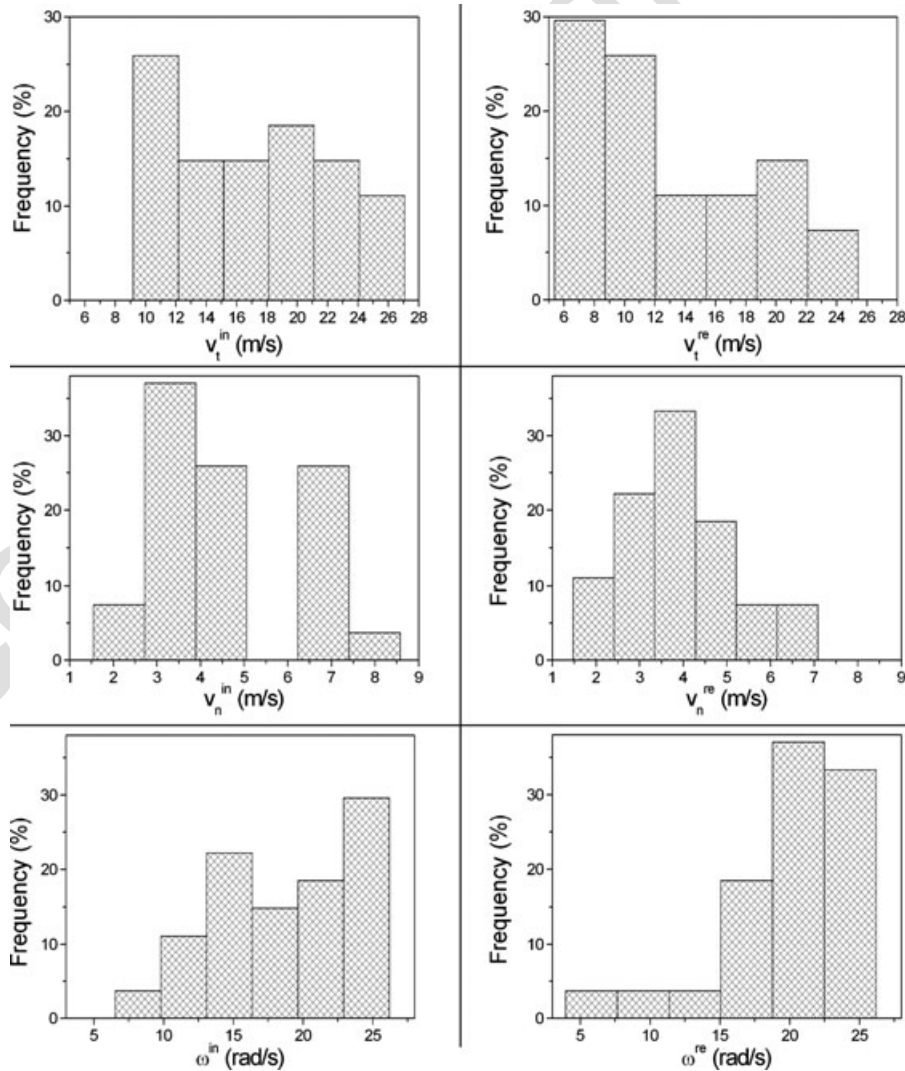|		Incident	Reflected
Mean values	v_t (m s⁻¹)	17.08	13.07
	v_n (m s⁻¹)	4.64	3.94
	ω (rad s⁻¹)	19.25	20.11
Standard deviations	v_t (m s⁻¹)	5.17	5.80
	v_n (m s⁻¹)	1.78	1.33
	ω (rad s⁻¹)	5.60	5.58

Figure 9. Distributions of the experimental incident and reflected velocities.

variation range of the tangential coefficient R_t^a is approximately from 0.7 to 1. The distribution of the apparent restitution coefficients measured in the present experiments is significantly different from these values (Figure 10). In particular, the normal coefficients at the gravity centre of the impacting rocks R_n^a are significantly larger (and reach above 1.0), whereas the measured tangential coefficient at the gravity centre of the impacting rocks R_t^a are in the same range as the classical values. Such differences were already observed in rockfall simulations using a stochastic impact model (Bourrier *et al.*, 2009a, 2009b). The observed differences with classical values were explained by the strong dependency of the apparent coefficients on the incidence angle. Consequently, one can deduce that the incidence angles observed in these experiments are significantly different from those in previous calibration experiments. Indeed, in these experiments, the incidence angles are very small (Figure 11) whereas most of the earlier calibration experiments generally consisted of vertical impacts of rocks on horizontal or inclined slopes, which induce larger incidence angles.

These important differences with the apparent restitution coefficients emphasize that the values of classical coefficients are valid only for nearly normal impacts. However, for shallow impact, which is the case in practice for steep slopes, these values are not valid if the restitution coefficients are directly applied to the gravity centre of the rocks. The effect of the rock shape should therefore be included in the rebound models, although in a very simple manner, as is the case in the lumped-mass model presented in this paper. Finally, one can note that in rebound models based on apparent restitution coefficients, the rotational velocity is not considered although it is a crucial parameter because the coupling between translational and rotational velocities is one of the causes of the observed differences in the apparent restitution coefficients (Bourrier *et al.*, 2009a).

Comparative analysis of the rebound models

The two numerical models were calibrated to obtain the best fit with the experimental results for all components of the reflected velocities. By trial and error approximation, the calibrated parameters for the two approaches were determined as shown in Table II.

Once calibrated, each of the two approaches can be used to calculate statistical distributions of the reflected velocities for a range of 'trial impacts'. The resulting distributions are shown in Figure 12 and the means and standard deviations of the resulting distributions are compared in Table III and Table IV. There is good agreement between the two simulation results and the experiments, when compared in terms of mean values. In terms
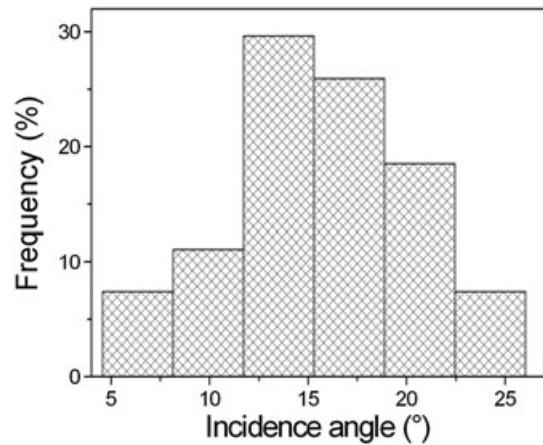

Figure 11. Distribution of the experimental incidence angles, defined as the angles between the incident velocities and the slope surface.

Table II. Values of the parameters of the lumped mass and of the rigid body models calibrated from the experimental results

Lumped mass	Rigid body
$M_{0.5} = 2 \times 10^3 \text{ kg m s}^{-1}$	$E = 50 \text{ MPa}$
$r_t = 0.9$	$v = 0.25$
$\alpha_l^{max} = 45°$	$r_k = 3$
$\varphi = 30°$	$\varphi_c = 30°$

of standard deviation, good agreement is seen only for the tangential velocities. The standard deviation of the normal velocities is significantly different for both approaches. This is due to the fact that both models induce many more small values for the normal reflected velocities whereas the distribution of the large values of this quantity is well predicted (Figure 12 and Figure 13). Finally, the rotational velocity standard deviation is not predicted by either of the approaches.

Comparisons of the cumulative distribution functions (Figure 13 and Figure 14) and of the probability distribution functions (Figure 12) for the different reflected velocities confirm these results. These results show that both models – based on four calibration parameters – allow simulation of all three components of the velocity changes in terms of mean values but differences are observed in the distribution of the values around the mean. The differences are significant for the rotational velocities and for the small values of the normal velocities.

The observed differences are first due to the methodology used for the choice of the experimental rebounds to be analysed. This choice can explain the overestimation of low
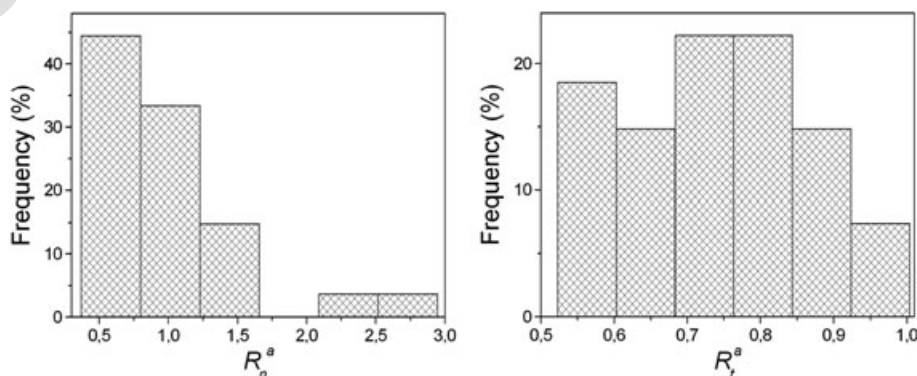

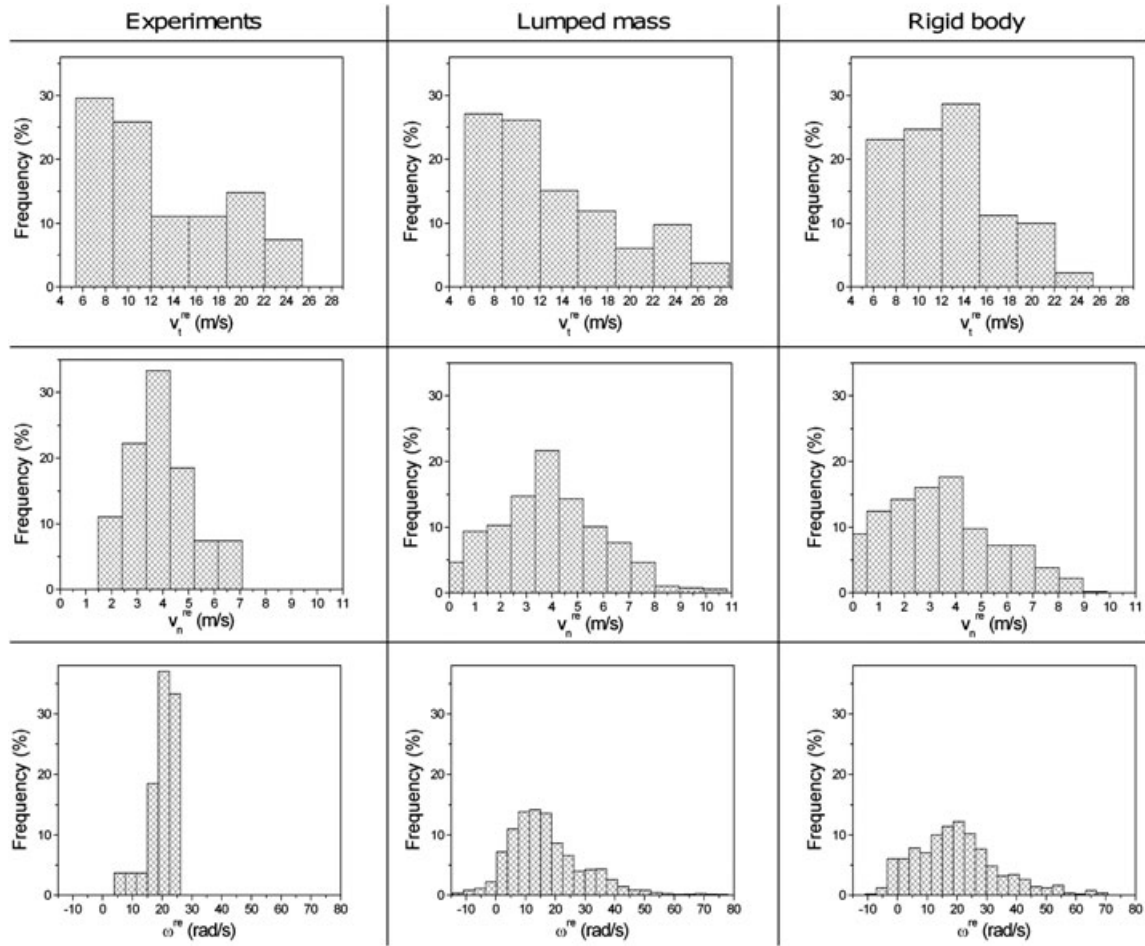**Figure 10.** Distributions of the apparent restitution coefficients.

Figure 12. Comparison between the experimental and simulated distributions of the reflected velocities.

Table III. Mean values and standard deviations of the experimental and simulated reflected velocities

		Experiments	Lumped mass	Rigid body
Mean values	v_t^{re} (m s^{-1})	13.07	13.07	12.61
	v_n^{re} (m s^{-1})	3.94	3.45	3.40
	ω^{re} (rad s^{-1})	20.11	16.77	19.95
Standard deviations	v_t^{re} (m s^{-1})	5.80	6.07	4.47
	v_n^{re} (m s^{-1})	1.33	2.39	2.13
	ω^{re} (rad/s)	5.58	13.42	14.38

Table IV. Relative errors on the mean values and standard deviations of the simulated reflected velocities

		Relative error (%)	
		Lumped mass	Rigid body
Mean values	v_t^{re}	0.00	−3.52
	v_n^{re}	−12.44	−13.71
	ω^{re}	−16.61	−0.80
Standard deviations	v_t^{re}	4.66	−22.93
	v_n^{re}	79.70	60.15
	ω^{re}	140.50	157.71

values of the normal velocities. The rebounds with very small normal velocities correspond to shallow impacts, where linear momentum is converted to rolling motion. Such rebounds were not analysed in the experiments because the rocks were nearly rolling and the impact points could therefore not be identified. They are therefore not accounted for in the experimental measures whereas they are predicted by the simulations.

Second, the limitations of both models can explain these differences. In particular, the deficiencies of the model can explain the poor prediction of the distributions of the rotational velocities.

For the lumped mass model, potential improvements to the models could consist in introducing the impact of a solid having a more complex shape, such as an ellipse for example, on a plane. However, even if analytical solutions may be found for such a problem (Goldsmith, 1960; Brogliato, 1999), several practical difficulties may arise when introducing such a model in a lumped mass rockfall simulation code. First, as lumped mass models only allow calculation of the trajectory of the gravity centre of the rocks, the precise detection of the impact point of an ellipse on the slope surface is difficult. Lumped mass models could, however, provide a rough estimate of the location of the impact point, which could be sufficient given the resolution of the digital terrain models, and calculate the rebound of the complex-shaped rock using the model mentioned previously. The second major difficulty that may be encountered is that the calculation of the rebound requires knowing the orientation of the complex-shaped rock just before impact which is currently not implemented into classical lumped mass approaches.

For rigid body approaches, the most promising and practicable improvements of the models to increase their predictive capacity could be to introduce a rolling resistance at the contact point to account for local shapes of the rocks and for
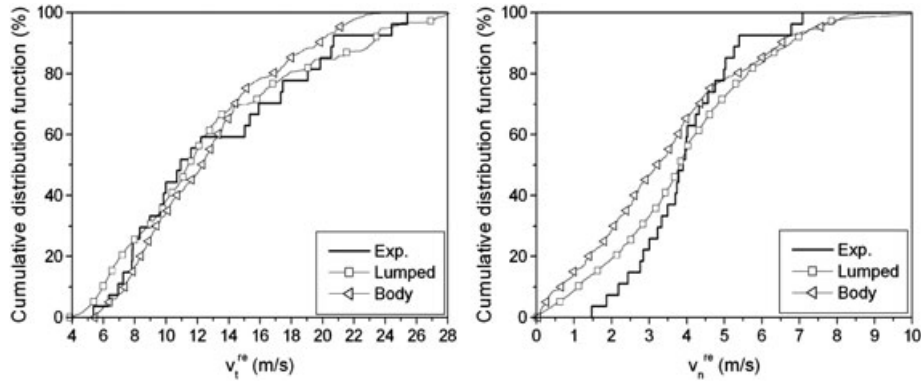
8

Figure 13. Comparison between the experimental and simulated cumulative distribution functions of the tangential and normal reflected velocity.
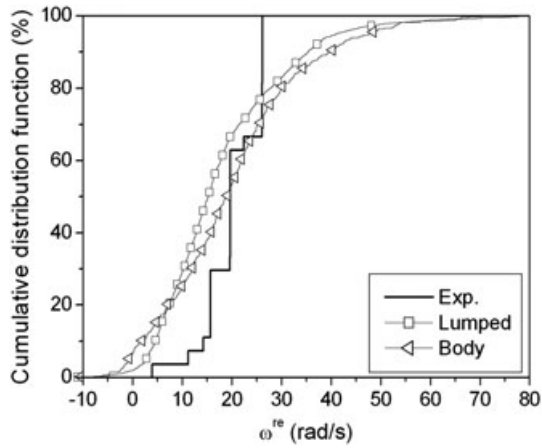

Figure 14. Comparison between the experimental and simulated cumulative distribution functions of the rotational reflected velocity.

soil strains in front of the rock that create an obstacle and consequently reduce the rotations.

Improvements of the models could also consist, for rigid body approaches, of using more complex rock shapes (polyhedron or more complex spheres assemblies), and, for lumped-mass approaches, of using non-uniform distributions of the slope perturbation angle (such as beta distributions, for example). However, the detailed information required for such rigorous analysis cannot practically be assembled and a certain simplification of the results must be accepted.

The different parameters of the two models can be classified by the role they play. The r_t and $M_{0.5}$ parameters of the lumped mass approach and the E, v, and r_k parameters of the rigid body approach can be associated with elasto-plastic energy dissipation. In addition, frictional energy dissipation is accounted for by the value of friction angles in both models. The local slope perturbation angle, which is the fourth calibration parameter used in the lumped-mass approach, does not correspond to any calibration parameter of the rigid body model. It can therefore be related with the other varying quantities in this approach: the shape and the orientation of the particle. The fact that both models approximate the experimental results clearly shows that the local slope perturbation angle used in the lumped mass algorithm represents not only the roughness of the soil, as classically mentioned, but also the effect of the shape and orientation of the rock. Therefore, this simple device can replace explicitly accounting for the shape of the particle, as required by the rigid body approaches.

Comparison between the predictions of the two models shows that the accuracies of both models are nearly similar. However, the rigid body approach relies on physical

parameters that can be measured in the field if required and allows direct calculation of the rebound in three dimensions. On the contrary, the parameters of the lumped-mass approaches are not easily related to field measurable quantities although it is possible to relate them to field relevant parameters following the approach described in Dorren *et al.* (2006) and Bourrier *et al.* (2009a, 2009b), for example. In addition, the use of lumped mass models in 3D rockfall simulations requires calculating the deviation angles of the rocks in the second phase of the rebound calculation (cf. Fig. 6). This parameter is very difficult to calibrate due to the reduced amount of information on it.

Finally, for both models, the variability of the results is mainly related with one probabilistic parameter assumed to be uniformly distributed. For the rigid body approach, this parameter is the orientation of the rock before impact for which the range of all possible values ($0° \leq \beta < 180$ °) was explored. For the lumped mass model, the slope perturbation angle is the statistical calibration parameter also assumed to be uniformly distributed. The assumption of uniform distribution appears to be valid based on these results. However, further testing is required, by comparing calculations and field results.

Conclusion

Analysis of local measurements of rock particle rebound in full-scale field tests yields values of apparent restitution coefficients that differ significantly from classical values cited in the literature. This result shows that the direct use of laboratory values is not well adapted and that the influence of the impact incidence angle, in particular, is very important.

Second, at the scale of the rebound, both lumped mass and rigid body approaches are efficient with only a few parameters. The accuracy of both of these approaches relies on the representative modelling of the energy dissipation and of the influence of shape as well as orientation of the particles. Rock shape is explicitly modelled in the rigid body approach whereas it is implicitly embedded in the lumped mass model by means of the local slope perturbation ('roughness') angle. Although the lumped mass approach allows the results to be fitted satisfactorily, its limitation is due to potential difficulties in calibrating the value of the roughness angle in practice. On the other hand, the accuracy of the rigid body approach relies on the correct estimation of rock length and height from field geological and historical analyses.

Finally, the observed discrepancies show that there is potential for further improvement. In particular, the prediction of the rotational velocities distribution could be improved by accounting for the local soil strains and the local shape of the rocks, both of which significantly condition the rebound

process. However, these improvements should be done in a pragmatic manner so that, despite the complexity of the model, the amount and accuracy of the required input data remain realistic.

References

An B, Tannant DD. 2007. Discrete element method contact model for dynamic simulation of inelastic rock impact. *Computers and Geosciences* **33**: 513–521.

Azzoni A, Barbera G, Zaninetti A. 1995. Analysis and prediction of rockfalls using a mathematical model. *International Journal of Rock Mechanics and Mining Sciences* **32**: 709–724.

Bourrier F, Dorren LKA, Nicot F, Berger F, Darve F. 2009a. Toward objective rockfall trajectory simulation using a stochastic impact model. *Geomorphology* **110**: 68–79.

Bourrier F, Eckert N, Nicot F, Darve F. 2009b. Bayesian stochastic modeling of a rock bouncing on a coarse soil. *Natural Hazards and Earth Systems Sciences* **9**: 831–846.

Bourrier F, Hungr O. 2011. Rockfall dynamics: a critical review of collision and rebound models. In *Rockfall Engineering: from Prediction to Mitigation*. Lambert S, Nicot F (eds). ISTE-John Wiley: London.

Bozzolo D, Pamini R. 1986. Simulation of rock falls down a valley side. *Acta Mechanica* **63**: 113–130.

Bozzolo D, Pamini R, Hutter K. 1988. Rockfall analysis - a mathematical model and its test with field data. *Landslides - Proceedings of the Fifth International Symposium on Landslides*, Lausanne, Switzerland; 555–560.

Brogliato B. 1999. *Nonsmooth Mechanics: Models, Dynamics, and Control*. Springer-Verlag: London.

Budetta P, Santo A. 1994. Morphostructural evolution and related kinematics of rockfalls in Campania (southern Italy): a case study. *Engineering Geology* **36**: 197–210.

Chau KT, Wong RHC, Lee CF. 1998. Rockfall problems in Hong Kong and some new experimental results for coefficients of restitution. *International Journal of Rock Mechanics and Mining Sciences* **35**(4–5): 662–663.

Chau KT, Wong RHC, Wu JJ. 2002. Coefficient of restitution and rotational motions of rockfall impacts. *International Journal of Rock Mechanics and Mining Sciences* **39**: 69–77.

Cundall P, Strack ODL. 1979. A discrete numerical model for granular assemblies. *Geotechnique* **29**: 47–65.

Descoeudres F, Zimmermann T. 1987. Three-dimensional dynamic calculation of rockfalls. *Proceedings of the Sixth International Congress on Rock Mechanics, International Society for Rock Mechanics*, Montreal, Canada; 337–342.

Dewez T, Nachbaur A, Mathon C, Sedan O, Kobayashi H, Rivière C, Berger F, Des Garets E, Nowak E. 2010. OFAI: 3D block tracking in a real-size rockfall experiment on a weathered volcanic rocks slope of Tahiti, French Polynesia. *Proceedings of the Rock Slope Stability Symposium INERIS*, Paris, France; 1–13.

Di Prisco C, Vecchiotti M. 2006. A rheological model for the description of boulder impacts on granular strata. *Geotechnique* **56**(7): 469–482.

Dimnet E, Fremond M. 2000. Instantaneous collisions of solids. *Proceedings of the European Congress on Computational Methods in Applied Sciences and Engineering*, Barcelona, Spain; 11–17.

Dorren LKA. 2003. A review of rockfall mechanics and modelling approaches. *Progress in Physical Geography* **27**(1): 69–87.

Dorren LKA, Berger F, Putters US. 2006. Real size experiments and 3D simulation of rockfall in forested and non-forested slopes. *Natural Hazards and Earth Systems Sciences* **6**: 145–153.

Evans S, Hungr O. 1993. The assessment of rockfall hazard at the base of talus slopes. *Canadian Geotechnical Journal* **30**: 620–636.

Fornaro M, Peila D, Nebbia M. 1990. Block falls on rock slopes - application of a numerical simulation program to some real cases. *Proceedings of the 6th International Congress IAEG*, Rotterdam, Netherlands; 2173–2180.

Frémond M. 1995. Rigid bodies collisions. *Physics Letters A* **204**: 33–41.

Giani GP. 1992. *Rock Slope Stability Analysis*. Balkema: Rotterdam.

Giani GP, Giacomini A, Migliazza M, Segalini A. 2004. Experimental and theoretical studies to improve rock fall analysis and protection work design rocks mechanics and rock engineering. *Rock Mechanics and Rock Engineering* **37**(5): 369–389.

Goldsmith W. 1960. *Impact: the Theory and Physical Behaviour of Colliding Solids*. Edward Arnold: London.

Guzzetti F, Crosta G, Detti R, Agliardi F. 2002. STONE: a computer program for the three dimensional simulation of rock-falls. *Computers and Geosciences* **28**: 1079–1093.

Kamijo A, Onda S, Masuya H, Tanaka Y. 2000. Fundamental test on restitution coefficient and frictional coefficient of rock fall. *Proceedings of the 5th Symposium on Impact Problems in Civil Engineering*, Japan; 83–86.

Kobayashi Y, Harp EL, Kagawa T. 1990. Simulation of Rockfalls triggered by earthquakes. *Rock Mechanics and Rock Engineering* **23**: 1–20.

Labiouse V, Heidenreich B. 2009. Half-scale experimental study of rockfall impacts on sandy slopes. *Natural Hazards and Earth Systems Sciences* **9**: 1981–1993.

Labiouse V, Heidenreich B, Desvarreux P, Viktorovitch M, Guillemin P. 2001. Etudes trajectographiques, Prévention des mouvements de versants et des instabilités de falaises. In Programme Interreg II C: 155–211.

Moreau JJ, Panagiotopoulos PD. 1988. *Non Smooth Mechanics and Applications*. Springer-Verlag: Wien.

Nicot F, Gotteland P, Bertrand D, Lambert S. 2007. Multi-scale approach to geo-composite cellular structures subjected to impact. *International Journal for Numerical and Analytical Methods in Geomechanics* **31**: 1477–1515.

Paronuzzi P. 1989. Probabilistic approach for design optimization of rockfall protective barriers. *Quaterly Journal of Engineering Geology* **22**: 175–183.

Pfeiffer T, Bowen T. 1989. Computer simulation of rockfalls. *Bulletin of the Association of Engineering Geologists* **26**(1): 135–146.

Piteau DR, Clayton R. 1977. Discussion of paper computerized design of rock slopes using interactive graphics for the input and output of geometrical data. *Proceedings of the 16th Symposium on Rock Mechanics*, Cundall P (ed). Minneapolis; 62–63.

Salciarini D, Tamagnini C, Conversini P. 2009. Numerical approaches for rockfall analysis: a comparison. *Proceedings of the 18th International Congress on Modelling and Simulation*, Cairns, Australia; 2706–2712.

Spang R, Rautenstrauch R. 1988. Empirical and mathematical approaches to rockfall protection and their practical applications. *Landslides - Proceedings of the 5th International Symposium on Landslides*, Lausanne, Switzerland; 1237–1243.

Spang R, Sonser T. 1995. Optimized rockfall protection by "Rockfall". *Proceedings of the 8th International Congress in Rock Mechanics*, Tokyo, Japan; 1233–1242.

Ushiro T, Shinohara S, Tanida K, Yagi N. 2000. A study on the motion of rockfalls on Slopes. *Proceedings of the 5th Symposium on Impact Problems in Civil Engineering*, Japan; 91–96.

Wu SS. 1985. Rockfall evaluation by computer simulation. *Transportation Research Record* **1031**: 1–5.